

Controlled formation of metallic nanowires via Au nanoparticle *ac* trapping

L. Bernard, M. Calame, S. J. van der Molen, J. Liao and C. Schönenberger

Institute of Physics, University of Basel, 4056 Basel, Switzerland

E-mail: michel.calame@unibas.ch

Abstract. Applying *ac* voltages, we trapped gold nanoparticles between micro-fabricated electrodes under well-defined conditions. We demonstrate that the nanoparticles can be controllably fused together to form homogeneous gold nanowires with pre-defined diameters and conductance values. Whereas electromigration is known to form a gap when a *dc* voltage is applied, this *ac* technique achieves the opposite, thereby completing the toolkit for the fabrication of nanoscale junctions.

PACS numbers: 73.23.-b, 73.40.Jn, 73.63.-b, 73.63.Rt, 81.07.-b, 81.07.Lk, 81.16.Rf

1. Introduction

Novel nanometer-scale electronic systems have been extensively developed during the last few years. For example, field-effect transistors made from carbon nanotubes [1] and organic molecules [2, 3] are being designed to constitute alternative routes to Si-based technology. Molecular electronics in particular combines several advantages: nanometer-scale size, flexibility of chemical synthesis and discrete energy levels. These aspects make molecules appear as promising building blocks for ultimate nano-electronics [4]. However, a key challenge within this size range remains the control of the connection between a few molecules and macroscopic current and voltage leads [5]. This requires the fabrication of contacts down to the size of a few nanometers. Electron-beam lithography can presently only hardly reach sub-10 nm resolution, or under very specific conditions [6, 7, 8]. Thus, new techniques need to be developed to produce nano-scale contacts. Among others, one philosophy is to start from e-beam prefabricated micro-electrodes and decrease the gap in a second step, for example via electrodeposition [9]. A promising method is to close the gap by metallic nanoparticles, used as intermediates, linking the molecules to the electrodes [10, 11, 12, 13, 14]. Hence, there is a need for the precise positioning of nanoparticles within larger structures.

A simple and controllable method to position nanoparticles is reported here. It consists of aligning and contacting colloids by means of dielectrophoresis (*ac* trapping) [15, 16, 17]. This technique has previously been used to manipulate a variety of micrometer- and nanometer-size objects including biopolymers [18, 19], cells [20] and metallic colloids [21, 22, 23, 10, 24, 25]. However, a systematic approach is still lacking. This is in particular true concerning the assembly of metallic particles in sub-micrometer gap sizes. In the present work, the process of *ac* trapping nanoparticles with diameters in between 10 nm and 100 nm into gaps of widths ranging from 20 nm to 500 nm has been investigated. Remarkably, the technique enables one to form continuous nanowires of tunable diameter between microfabricated electrodes. This process can be initiated by choosing the proper *ac* voltage and series impedance.

2. Experimental

Pairs of planar, tip-shaped gold (Au) electrodes facing each other were patterned on a Si/SiO₂ substrate using conventional UV and electron-beam lithography (EBL). Before each fabrication step, the substrate was cleaned in acetone, followed by isopropanol and was finally exposed to an oxygen plasma for 5 min. After resist spinning, exposure and development, a 5 nm thick adhesion layer of Ti was deposited prior to the evaporation of a 35 nm Au layer. The tips of the electrodes pairs were separated by a gap typically ranging between 20 and 100 nm. Using an angle evaporation technique, the gap size can be reduced to less than 20 nm, however with a relatively small yield (~5%).

Colloidal solutions of charge-stabilised Au particles were prepared following the method of Turkevich *et al.* [26]. A 0.5 mM solution of $HAuCl_4$ was reduced with aqueous

citric acid at boiling temperature. This resulted in nearly monodisperse charge-stabilised Au colloids with a diameter between 10 nm and 30 nm, depending on the reducing agent concentration. Using these charge-stabilised Au colloids as the starting material, we have also prepared alkane-thiol encapsulated Au colloids following the method of Huang *et al.* [27]. For subsequent experiments, the encapsulated colloidal particles were dissolved in a 1 : 1 mixture of hexane and dichloromethane.

Trapping of the Au nanoparticles was performed via dielectrophoresis (DEP) by applying an *ac* electric field \vec{E} between the two electrodes. The dielectrophoretic force \vec{F}_{DEP} acting on a homogeneous, isotropic particle of radius a is proportional to the gradient of the electric field amplitude squared and reads [17]:

$$\vec{F}_{DEP} = \pi a^3 \epsilon_m \cdot \Re \left[\frac{\tilde{\epsilon}_p - \epsilon_m}{\tilde{\epsilon}_p + 2\epsilon_m} \right] \cdot \vec{\nabla} |\vec{E}|^2$$

where \Re denotes the real part. The effective polarizability of the particle in the medium is expressed by the relative permittivities of the particle $\tilde{\epsilon}_p$ and the medium ϵ_m . This force typically ranges from 0.1 pN to 1 pN [16, 17].

A circuit diagram of our setup is sketched in Figure 1. The scheme includes a series capacitor C_s and a series resistor R_s , which constitute a total series impedance Z_s . The capacitor was placed in the circuit to filter out any *dc* component and to avoid electrochemical processes or electromigration [28]. It also prevented further effects due to, for instance, the electrophoretic mobility of the ionic solution, which can influence the motion of the suspended nanoparticles. To measure the time-dependence of the current, $i(t)$, we recorded the voltage drop over R_s . For this, both a time-averaging lock-in amplifier and a fast digital oscilloscope were used. The lock-in amplifier continuously monitored the trapping process with a time-resolution of ≈ 100 ms. In contrast, the oscilloscope, which provided a much faster time resolution of ≈ 100 ns, was adjusted to trigger at the trapping event, when a significant increase of the current amplitude \hat{I} was monitored. In this way we measured the delay time until a particle is trapped and the temporal evolution of the impedance during junction formation. In order to limit the number of parameters in the process, we fixed the frequency f of the *ac* field throughout the trapping experiments to a value of 1 MHz. This allowed the manipulation of nanoparticles with diameters ranging between 10 nm and 100 nm at concentrations of order 10^{13} mL $^{-1}$. Typical values for the total input voltage V_{in} and the series resistor R_s were $V_{in} \leq 3.5$ V and $0 \Omega \leq R_s \leq 500 \Omega$, respectively. Throughout this paper, the symbols I , V , R and P refer to the RMS values of the current, voltage, resistance and dissipation at (in) the junction, respectively. During the trapping process, they are time dependent. Their final values, once the trapping is completed, are denoted by I_f , V_f , R_f and P_f , respectively.

3. Results and discussion

We explored various types of colloids with a main focus on charge-stabilised Au colloids with a diameter of 25 ± 5 nm. To investigate the trapping process in detail, the current

through 103 junctions was measured during and after the trapping of these specific particles. All samples were prepared following the same procedure. Figure 2A shows a typical lock-in measurement of the current I flowing through a junction during trapping. First, a colloidal solution droplet was deposited on the device ($t < 0$). Next, an ac trapping voltage V_{in} was applied at $t = 0$ to attract the nanoparticles to the junction. This gave rise to a detectable leakage current through the solution (arrow 1). After the duration t_1 of typically a few seconds to one minute, a large current increase was suddenly observed (arrow 2). This event signals the formation of a conducting bridge within the gap due to the trapping of individual nanoparticles. The conductance jump takes place when the last nanoparticle gets trapped and completes the closing of the gap. After this increase, the current remained constant and finally, the input voltage V_{in} was set to zero (arrow 3). We note that in a few particular cases the current did not increase in a single step, but rather displayed multiple steps, suggesting the formation of a few conducting bridges in parallel. Figure 2B shows a typical oscilloscope trace of $i(t)$, set up to trigger exactly at the current increase (arrow 2, Figure 2A). We see that the junction changes its resistance typically within $t_2 \sim 1 \mu s$. Figure 2C shows the dependence of the average trapping time t_1 on the voltage over the junction V (for $t < t_1$). The trapping time roughly scales with the inverse of the voltage squared $1/V^2$, which agrees with the expectation for a driven particle movement impeded by viscous friction. In that case the velocity scales with the driving force which is, according to the expression for the dielectrophoretic force, proportional to the electric field squared, and hence to the voltage squared.

After each trapping experiment, scanning-electron microscopy (SEM) inspection of the samples revealed that in 67 cases the junctions showed no sign of breakdown. Figure 3 reports a set of representative results. First, we focus on Figures 3A and 3B. Here, nanoparticles with a relatively large diameter of 120 ± 20 nm were trapped into ~ 500 nm large gaps. The trapping conditions for both cases were identical, except for the applied voltage V_{in} : 2 V in case A and 1 V in case B. We clearly observe a larger number of trapped particles in A than in B. This illustrates that one can tune the number of nanoparticles bridging the gap by adjusting the trapping voltage. The electric field required for optimal trapping amounts to about $E \approx 10^7$ V/m. In Figure 3B, a well-ordered chain of nanoparticles was formed with a junction resistance of *only* 50Ω . This is surprising and indicates that after the nanoparticles were trapped, a second, ‘anchoring’ process took place. During anchoring, the colloids become physically and electrically connected, leading to a low final resistance. Figure 3C shows a device in which even smaller particles, i.e. 25 ± 5 nm, were trapped, with an applied voltage $V_{in} = 1$ V. Remarkably, the individual colloids are not distinguishable any longer. Instead of building a chain, as in Figure 3B, the particles have fused together forming a *wire* with a well defined diameter. The final resistance of this wire is comparatively low, i.e. 160Ω . Figure 3 shows that the anchoring process can lead to the formation of two distinct structures: chains or wires. Below, we will discuss this phenomenon in more detail. Finally, in Figure 3D and E, we show examples of junctions with relatively large final resistances

in the $M\Omega$ range. In Figure 3D, a single nanoparticle (25 ± 5 nm) was trapped. In contrast to Figures 3A-D where charge-stabilised colloids were used, Figure 3E shows a typical result for the trapping of dodecanethiol ($C_{12}H_{25}S$)-functionalized nanoparticles of 10 nm diameter within a 30 nm gap. Unlike the former cases, devices made with functionalized particles never displayed fusing and the resistance values were always large ($> M\Omega$).

In 11 cases of the 67 successful trapping experiments with 25 ± 5 nm diameter charge-stabilised nanoparticles, the final junction resistance R_f was much larger than $1 M\Omega$. This indicates that no metallic contact was established between the nanoparticles and the electrodes. An overview of the rest of the data set (56 experiments) is given in Figure 4. Here, we plot the final device resistance R_f as a function of the current I_f , both measured at the end of the trapping and anchoring process. There is quite some scatter in the final resistance of the devices. Nevertheless, the data set is confined between a lower and an upper bound given by the voltage $V_f = I_f R_f$. More precisely, the voltage over the junction always lies in between 0.2 V and 1.6 V, as indicated by the dotted lines, a typical value being 0.9 V. The lower bound in Figure 4 is related to the trapping process: if the electric field is too small, trapping does not take place. In contrast, a voltage that is too large leads to sample destruction after trapping as evidenced by ‘burnt’ electrodes which are modified on a macroscopic scale. This breakdown process is likely related to a thermal run-away by excessive Joule heating as reported in electromigration experiments on nanojunctions [29, 30, 31]. The open and solid data points in Figure 4 relate to two different kinds of junctions. The solid dots refer to junctions in which the nanoparticles formed chains during the trapping process (cf. Figure 3B), whereas the open dots relate to wire formation (cf. Figure 3C). It appears that the two subsets group together in Figure 4, despite the clear scatter. Hence, Figure 4 forms a good basis to discuss about the possible processes behind anchoring, chain and wire formation, as well as device breakdown.

We first focus on the moment when a set of nanoparticles is being trapped in the junction at $t = t_1$. These particles experience a large electric field in the gap region $\sim 10^7$ V/m, which induces a dipole in each of them. Consequently, the dipole-dipole interaction between the particles becomes significant, tending to line up the particles in the junction. This explains the preference for the initial chain formation. At that point, the charge-stabilised particles are not yet interconnected, so that the whole voltage drops over the tiny gaps (≤ 1 nm) between the particles. This has two consequences. First, the electric field is much more localised than before chain formation. Hence, the range of the DEP force is decreased, leading to a much smaller trapping probability for left-over particles in the solution. In this way, DEP is self-limiting. Second, the field over the gaps between the individual colloids tend to become very high, $\geq 10^8$ V/m. At such fields, surface diffusion of Au atoms is enhanced in the direction of the gap and can lead to the formation of narrow Au bridges between the nanoparticles [32, 33]. If no connections are formed, a device will have a high final resistance ($\gg 1 M\Omega$), as observed in 11 of our 71 junctions made with charge-

stabilised particles. As mentioned above, junctions prepared with alkanethiol-covered particles *always* yielded high resistance values, suggesting that the alkanethiol shell protects the colloids against field-driven atomic migration. However, in most devices with charge-stabilised particles, the particles were interconnected and the resistance of the devices dropped dramatically. One may wonder what determines the final value R_f of these junctions. To address this point, we refer to Figure 5A, where a histogram of $\log(R_f/|Z_s|)$ is plotted. This graph describes the probability distribution of the ratio of R_f to the total series impedance $|Z_s|$. We find that R_f is typically of the same order of magnitude as $|Z_s|$. The histogram features a clear peak with a maximum around a ratio of $\log(R_f/|Z_s|) = 0.2$, corresponding to $R_f = 1.6|Z_s|$. In the inset of Figure 5A, we show a stacked bar plot of the percentage of chains (dark) and wires (light) for three ranges of $|Z_s|$. Interestingly, chains are more common for higher $|Z_s|$, while wires are mostly found for lower $|Z_s|$. Figure 5A indicates that we can tune (at least roughly) the device properties via the series impedance.

To understand this, we bring forward a possible model of wire formation. We first note that a change in shape from chain to wire leads to a decrease of the total surface energy. Hence, we expect that surface tension is the effective driving force for the fusing process. Also, in order to transform a chain of spherical particles into a rod-like wire, a considerable diffusion of Au atoms is needed. Since diffusion is an activated process, an increase of the junction temperature by Joule heating will clearly facilitate wire formation. Before fusing, $R \gg |Z_s|$ and the junction is voltage-biased with the power P dissipated over the junction given by $P = V_{in}^2/R$. Once atomic diffusion sets in and the gaps start to fill up, the resistance decreases and consequently the dissipation increases. If the applied voltage V_{in} is too large, this can lead to a thermal run-away and sample breakdown. However, the series impedance Z_s also has an effect on P . It can self-limit the thermal run-away process for moderate V_{in} . To see this, we note that the junction would be current-driven in the opposite regime $R \ll |Z_s|$. In that case, the local dissipation P is given by $P \approx RI^2$ and decreases with decreasing R , thus limiting the fusion process. The full dependence of P on $R/|Z_s|$ is shown in the inset of Figure 5B. There is a maximum power $P_{max} = V_{in}^2/4|Z_s|$ at $R = |Z_s|$. The dashed and dotted lines indicate the dissipation in the limiting cases of effectively current-biased and voltage-biased junctions, respectively. Based on this consideration, we expect the process to stop when $R \approx Z_s$ where the dissipation P reaches its maximum. Hence, the final dissipation P_f , measured at the end of successful junction formation, should be close to P_{max} . In Figure 5B, we display a histogram of P_f/P_{max} for all data points in Figure 4. For the vast majority of our devices, Figure 5B shows that $P_f \approx P_{max}$, as anticipated. Because the final resistance R_f is generally a bit larger than $|Z_s|$ (Figure 5A), we infer that the process tends to stop to the right of the maximum in the inset of Figure 5B.

Relating the junction temperature T to the power P is not straightforward, but it can be stated that T is related to the volume power density p . If we assume for simplicity that only the junction cross-section A changes during wire formation, but not its length L , we have $p := P/AL$. Because $R \propto 1/A$ one may also write $p \propto PR$. Hence,

in the beginning, when $R \gg |Z_s|$ and $P = V_{in}^2/R$, the power density is constant, even if A increases due to the thermally driven diffusion of Au atoms. This homogenization process can therefore go on at constant temperature until the assumption $R \gg |Z_s|$ is no longer valid. Then, p and hence T will decrease, limiting atomic diffusion. This picture suggests that the homogenisation process can proceed further for small $|Z_s|$ as compared to large $|Z_s|$. It therefore becomes understandable why wire-like devices appear for small $|Z_s|$, whereas chain-like ones appear for large $|Z_s|$, consistent with the inset of Figure 5A.

In the previous discussion, electromigration was ignored, since it does not occur for the *ac* current densities we apply [28]. In fact, electromigration at similar *dc* current densities leads to gap formation [2, 3, 31], which is the *opposite* effect compared to the new ‘gap-closing’ process that we report here. Interestingly, the series impedance and Joule heating play a similar role in electromigration experiments as in the work presented here [31]. We speculate that repeated gap formation and closing should be possible by using *ac* and *dc* voltages, alternately.

4. Conclusions

We demonstrate a simple method to control the formation of metallic nanowires and chains of desired length and diameter. It is based on the dielectrophoretic trapping of nanoparticles. We point out the relevance of two processes: the trapping and the subsequent anchoring of the particles between the electrodes. By choosing a proper series impedance, one can tune the final resistance and appearance of a junction: lower series impedances favor wire formation, whereas higher series impedances result in chains. The nanostructures produced are promising elements in the framework of nanoelectronics. For instance, they can be used to contact nanometer-size building blocks, possibly in combination with *dc* electromigration. Using this approach, it may become possible to fine tune nanogaps in electromigration devices, which is of high interest to molecular electronics.

Acknowledgments

We are grateful to M. Steinacher for his technical support. S.J.vd M. acknowledges the Netherlands Organisation for Scientific Research, NWO (‘Talent stipendium’). This work was supported by the Swiss National Science Foundation, the Swiss National Center of Competence in Research “Nanoscale Science” and the European Science Foundation through the Eurocore program on Self-Organised Nanostructures (SONS).

References

- [1] S.J. Wind, J. Appenzeller, R. Martel, V. Derycke, and Ph. Avouris. Vertical scaling of carbon nanotube field-effect transistors using top gate electrodes. *Appl. Phys. Lett.*, 80:3817–3819, 2002.

- [2] W. Liang, M.P. Shores, M. Bockrath, J.R. Long, and H. Park. Kondo resonance in a single-molecule transistor. *Nature*, 417:725–729, 2002.
- [3] H.S.J. van der Zant, Y.-V. Kervennic, M. Poot, K. O'Neill, Z. de Groot, J.M. Thijssen, H.B. Heersche, N. Stuhr-Hansen, T. Bjørnholm, D. Vanmaekelbergh, C.A. van Walreed, and L.W. Jenneskens. Molecular three-terminal devices: fabrication and measurements. *Faraday Discuss.*, 131:347–356, 2006.
- [4] J.R. Heath and M.A. Ratner. *Physics Today*, 56:43–49, 2003.
- [5] K.W. Hipps. *Science*, 294:536–537, 2003.
- [6] K. R. V. Subramanian, M. S. M. Saifullah, E. Tapley, D.-J. Kang, M. E. Welland, and M. Butler. Direct writing of ZrO₂ on a sub-10 nm scale using an electron beam. *Nanotechnology*, 15:158–162, 2004.
- [7] K. Liu, Ph. Avouris, J. Bucchignano, R. Martel, and S. Sun. Simple fabrication scheme for sub-10 nm electrode gaps using electronbeam lithography. *Appl. Phys. Lett.*, 80:865–867, 2002.
- [8] P. Steinmann and J. M. R. Weaver. Nanometer-scale gaps between metallic electrodes fabricated using a statistical alignment technique. *Appl. Phys. Lett.*, 86:063104, 2005.
- [9] A.F. Morpurgo, C.M. Marcus, and D.B. Robinson. Controlled fabrication of metallic electrodes with atomic separation. *Appl. Phys. Lett.*, 74:2084–2086, 1999.
- [10] AS.I. Khondaker and Z. Yao. *Appl. Phys. Lett.*, 81:4613–4615, 2002.
- [11] T. Dadoosh, Y. Gordin, R. Krahne, I. Khivrich, D. Mahalu, V. Frydman, J. Sperling, A. Yacoby, and I. Bar-Joseph. Measurement of the conductance of single conjugated molecules. *Nature*, 436:677–680, 2005.
- [12] D. P. Long, C. H. Patterson, M. H. Moore, D. S. Seferos, G. C. Bazan, and J. G. Kushmerick. Magnetic directed assembly of molecular junctions. *Appl. Phys. Lett.*, 86:153105, 2005.
- [13] J. Liao, L. Bernard, M. Calame, and C. Schönenberger. Reversible formation of molecular junctions in twodimensional nanoparticle arrays. *Adv. Mater.*, 18:2444–2447, 2006.
- [14] C. Xu, H. van Zalinge, J.L. Pearson, A. Glidle, J.M. Cooper, D.R.S. Cumming, W. Haiss, J.L. Yao, D.J. Schiffrin, M. Proupin-Pérez, R. Cosstick, and R.J. Nichols. A combined top-down bottom-up approach for introducing nanoparticle networks into nanoelectrode gaps. *Nanotechnology*, 17:3333–3339, 2006.
- [15] H.A. Pohl. *Dielectrophoresis*. Cambridge University Press, 1978.
- [16] T.B. Jones. *Electromechanics of particles*. Cambridge University Press, 1995.
- [17] H. Morgan and N.G.Green. *AC electrokinetics*. Research Studies Press; Baldock, England., 2003.
- [18] M. Washizu, S. Suzuki, O. Kurosawa, T. Nishizaka, and T. Shinoara. *IEEE Trans. Ind. Appl.*, 30:835–843, 1994.
- [19] F. Dewarrat, M. Calame, and C. Schönenberger. *Single Molecules*, 3:189–193, 2002.
- [20] R. Pethig and G.H. Marx. *Trends in Biotech.*, 15:426–432, 1997.
- [21] A. Bezryadin, C. Dekker, and G. Schmid. Electrostatic trapping of single conducting nanoparticles between nanoelectrodes. *Appl. Phys. Lett.*, 71:1273–1275, 1997.
- [22] K.D. Hermanson, S.O. Lumsdon, J.P. Williams, E.W. Kaler, and O.D. Veley. *Science*, 294:1082–1086, 2001.
- [23] I. Amlani, A.M. Rawlett, L.A. Nagahara, and R.K. Tsui. *Appl. Phys. Lett.*, 80:2761–2763, 2002.
- [24] R. Kretschmer and W. Fritzsche. Pearl chain formation of nanoparticles in microelectrode gaps by dielectrophoresis. *Langmuir*, 20:11797–11801, 2004.
- [25] S. O. Lumsdon and D. M. Scott. Assembly of colloidal particles into microwires using an alternating electric field. *Langmuir*, 21:4874–4880, 2005.
- [26] J. Turkevich, P.C. Stevenson, and J. Hillier. *Discuss. Faraday Soc.*, 11:55–75, 1951.
- [27] S. Huang, G. Tsutsui, H. Sakaue, S. Shingubara, and T. Takahagi. *J. Vac. Sci. Technol. B*, 19:115–120, 2001.
- [28] K.P. Rodbell, A.J. Castellano, and R.I Kaufman. Ac electromigration (10mhz-1mhz) in Al metallization. *AIP Conf. Proc.*, 418:212–223, 1998.
- [29] C. Durkan, M. A. Schneider, and M. E. Welland. Analysis of failure mechanisms in electrically

- stressed Au nanowires. *J. Appl. Phys.*, 86:1280–1286, 1999.
- [30] M.F. Lambert, M.F. Goffman, J.P. Bourgoin, and P. Hesto. *Nanotechnology*, 14:772–777, 2003.
- [31] M. L. Trouwborst, S. J. van der Molen, and B. J. van Wees. The role of joule heating in the formation of nanogaps by electromigration. *Journal of Applied Physics*, 99:114316, 2006.
- [32] T.T. Tsong. Effects of electric field in atomic manipulations. *Physical Review B*, 44:13703–13710, 1991.
- [33] J. Méndez, J. Gómez-Herrero, J.I. Pascual, J.J. Sáenz, J.M. Soler, and A.M. Baró. Diffusion of atoms on Au(111) by the electric field gradient in scanning tunneling microscopy. *J. Vac. Sci. Technol. B*, 14:1145–1148, 1996.

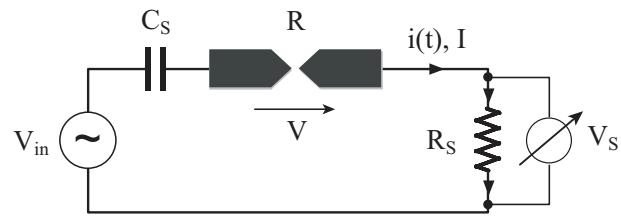


Figure 1. Schematics of the trapping circuit. Both an oscilloscope and a lock-in amplifier record the voltage drop V_s over the series resistor R_s . Together, R_s and the series capacitor $C_s = 1.5$ nF form the total series impedance Z_s .

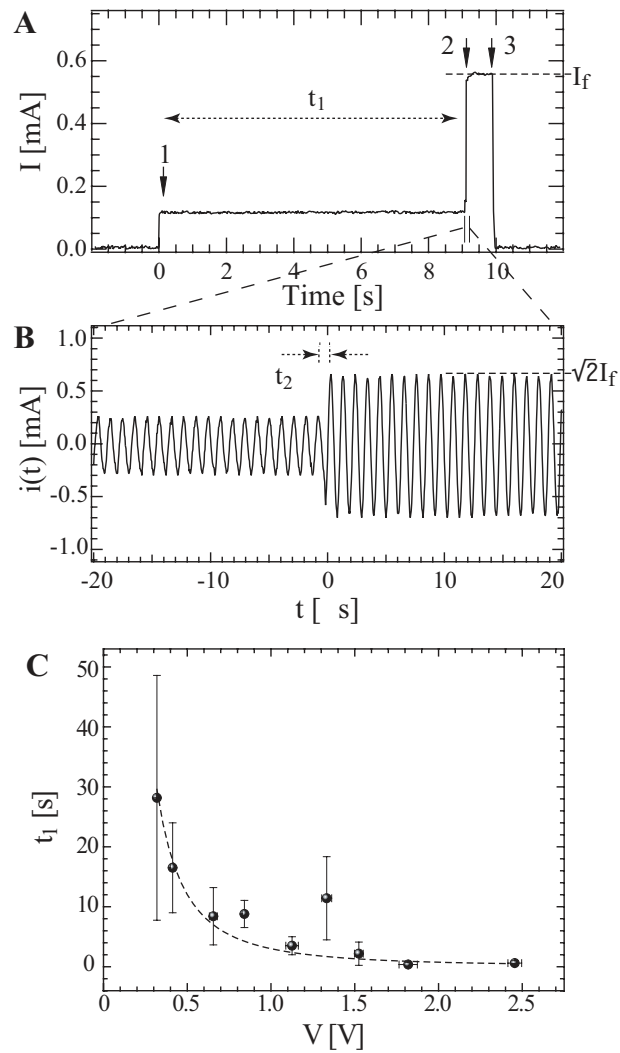


Figure 2. **A.** Typical record of the rms current I through the junction during both trapping and anchoring processes, with $V_{in} = 1$ V and series impedance $|Z_s| = 467 \Omega$. Arrows 1, 2 and 3 mark the time when the voltage was applied, the contact was made and the voltage was set to 0, respectively. The characteristic time for trapping, t_1 , is defined as the time between arrows 1 and 2. **B.** Close-up view of the ac current $i(t)$ measured with an oscilloscope around the contacting event ($t = 0$). **C.** t_1 as a function of the voltage over the junction V (at $t < t_1$). Each point is an average over several data points; the error bars correspond to the standard error. The dotted line represents a $1/V^2$ dependence.

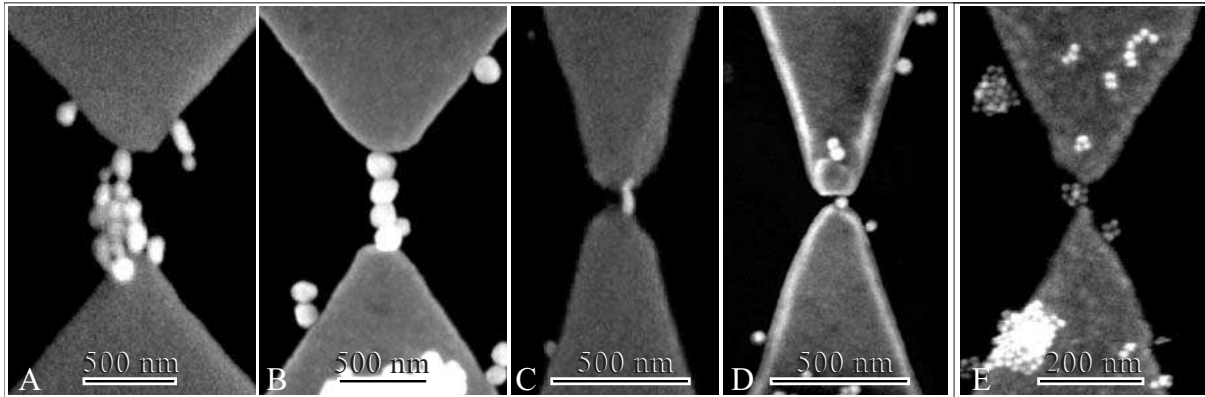


Figure 3. Scanning electron micrographs of junctions prepared under various conditions. **A.** Large gap (500 nm) with large nanoparticles (120 ± 20 nm) : parameters $V_{in} = 2$ V, $|Z_s| = 111 \Omega$; final resistance $R_f = 280 \Omega$. **B.** Large gap (560 nm) with large nanoparticles (120 ± 20 nm) : $V_{in} = 1$ V, $|Z_s| = 111 \Omega$; $R_f = 50 \Omega$. **C.** Small gap (40 nm) with a wire formed by small nanoparticles (25 ± 5 nm) : $V_{in} = 1$ V, $|Z_s| = 148 \Omega$; $R_f = 160 \Omega$. **D.** Small gap (30 nm) with a single small nanoparticle (25 ± 5 nm) : $V_{in} = 1.8$ V, $|Z_s| = 467 \Omega$; $R_f = 4.8$ M Ω . **E.** Small gap (20 nm) with small C_{12} -functionalized nanoparticles (10 ± 1 nm) : $V_{in} = 1$ V, $|Z_s| = 147 \Omega$; $R_f = 4$ M Ω .

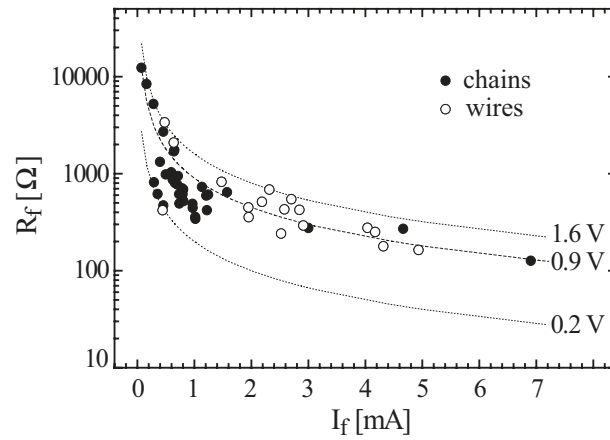


Figure 4. Final resistance R_f versus current I_f of the junctions showing successful trapping and anchoring (56 devices). The voltage over the junctions $V_f = I_f R_f$ is bound by 0.2 V from below (no trapping) and 1.6 V from above (breakdown after trapping), as indicated by dotted lines. A typical voltage is 0.9 V (dashed line). Solid dots: chain formation; open dots: wire formation (as extracted from SEM images).

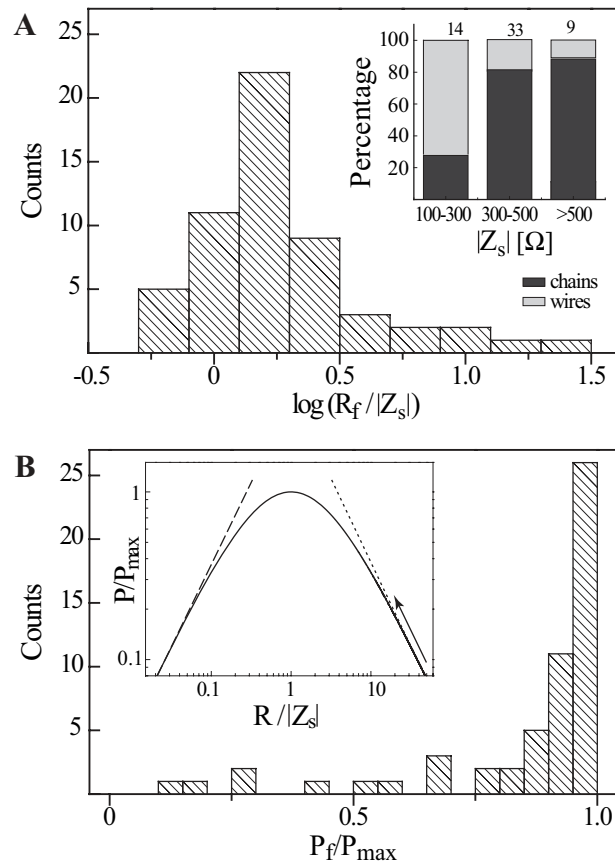


Figure 5. **A.** Histogram of $\log(R_f/|Z_s|)$, for the data in Figure 4. A single peak is seen with a maximum around $\log(R_f/|Z_s|) = 0.2$. The inset shows the percentage of chains (dark) and wires (light) for different values of $|Z_s|$. Wires are more favorably formed for lower $|Z_s|$. **B.** Histogram of P_f/P_{max} , where $P_f = V_f^2/R_f$. A clear majority of the devices has $P_f \approx P_{max}$. The inset shows a calculation of P/P_{max} as a function of $R/|Z_s|$, which reaches its maximum at $R = |Z_s|$ (Calculation for $Z_s = 452 - 134i\Omega$). The arrow indicates that the resistance of our junctions decreases during homogenisation. The dashed and dotted lines refer to the limiting cases of current- and voltage biasing, respectively.